Atmos. Chem. Phys. Discuss., 4, 8579–8607, 2004
www.atmos-chem-phys.org/acpd/4/8579/
SRef-ID: 1680-7375/acpd/2004-4-8579
European Geosciences Union

Atmospheric Chemistry and Physics Discussions

Nitric acid trihydrate (NAT) formation at low NAT supersaturations

C. Voigt[1], H. Schlager[1], B. P. Luo[2], A. Dörnbrack[1], A. Roiger[1], P. Stock[1], J. Curtius[3], H. Vössing[3], S. Borrmann[3,4], S. Davies[5], P. Konopka[6], C. Schiller[6], G. Shur[7], and T. Peter[2]

[1]Institut für Physik der Atmosphäre (IPA), DLR Oberpfaffenhofen, D-82234 Wessling, Germany
[2]Institut für Atmosphäre und Klima, ETH Zürich, Hönggerberg HPP, CH-8093 Zürich, Switzerland
[3]Institut für Physik der Atmosphäre, Universität Mainz, D-55099 Mainz, Germany
[4]Max-Planck-Institut für Chemie, D-55128 Mainz, Germany
[5]School of Environment, University of Leeds LS9JT, UK
[6]Forschungszentrum Jülich, ICG-I, D-52425 Jülich, Germany
[7]Central aerological observatory, Moscow, reg. 141700, Russia

Received: 8 December 2004 – Accepted: 8 December 2004 – Published: 23 December 2004

Correspondence to: C. Voigt (christiane.voigt@dlr.de)

Abstract

A polar stratospheric cloud (PSC) was observed on 6 February 2003 in the Arctic stratosphere by in-situ measurements onboard the high-altitude research aircraft Geophysica. Low number densities ($\sim 10^{-4}$ cm^{-3}) of nitric acid (HNO_3) containing particles – probably NAT – with diameters up to 6 μm were measured at altitudes between 18 and 20 km. These particles have the potential to grow further and to remove HNO_3 from the stratosphere, thereby enhancing polar ozone loss. Interestingly, the NAT particles formed in less than a day at temperatures $T > T_{NAT} - 3.5$ K, just slightly below the NAT equilibrium temperature T_{NAT}. This unique measurement of PSC formation at extremely low NAT saturation ratios ($S_{NAT} \lesssim 11$) constrains current NAT nucleation theories. In particular, NAT formation on ice can for certain be excluded. Conversely, we suggest that meteoritic particles may be favorable candidates for triggering nucleation of NAT at the observed low number densities.

1. Introduction

PSCs form in the winter polar stratosphere at low temperatures by uptake of water and nitric acid into stratospheric sulfate aerosol (Carslaw et al., 1994; Schreiner et al., 1999; Voigt et al., 2000b). At temperatures below the frost point T_{ICE} (~190 K), ice can nucleate in the supercooled ternary solution (STS) droplets (Koop et al., 2000), and the cloud may become visible as colourful iridescent ice PSC. PSCs consisting of NAT particles (Voigt et al., 2000a) have been detected in a broad size and number density range. High number densities ($n > 10^{-2}$ cm^{-3}) of small NAT particles ($d \leq 6$ μm) have been measured on small horizontal scales of some hundred square kilometers in cold regions induced by mountain waves (Carslaw et al., 1998; Wirth et al., 1999; Toon et al., 2000; Voigt et al., 2003). These dense PSCs provide sites for heterogeneous reactions that activate halogen species (Peter, 1997) leading to polar ozone destruction. In contrast, low number densities ($n \sim 10^{-4}$ cm^{-3}) of large nitric acid containing parti-

ACPD

4, 8579–8607, 2004

cles ($10\,\mu m < d < 20\,\mu m$) have been detected in synoptic-scale PSC fields (Fahey et al., 2001; Northway et al., 2002). Those large NAT particles can sediment and transport HNO_3 to lower altitudes (Fahey et al., 1990; Waibel et al., 1999). Under denitrified conditions, the passivation of active halogen species may be slowed down, thereby enhancing ozone loss.

Here we present measurements and simulations of small ($d < 6\,\mu m$) nitric acid containing particles at low particle number density ($n \sim 1.6 \times 10^{-4}\,cm^{-3}$). If these particles grow to larger sizes, they could provoke denitrification and enhanced polar ozone depletion. In contrast to previous measurements, conditions of particle formation can be precisely confined: the air parcels have spent less than a day at temperatures 0 to 3.5 K below T_{NAT}. This corresponds to NAT saturation ratios $S_{NAT} \lesssim 11$, where S_{NAT} is the ratio between the HNO_3 partial pressure and the HNO_3 vapor pressure of NAT. An exposure to temperatures below T_{ICE} can be excluded. How have these NAT particles formed? Besides current NAT nucleation theories, we investigate the effect of NAT nucleation on meteoritic particles.

2. Arctic winter 2002/2003

The Arctic stratosphere was extremely cold in early winter 2002/2003 with temperatures persistently below T_{NAT} between end of November and mid-January 2003. During this period, PSC formation over large areas influenced the chemical evolution of the polar vortex and led to denitrification of up to 50% (Schlager et al., in preparation, 2004[1]; Grooß et al., 2004). Processing of halogen species on PSC particles as well as denitrification finally resulted in ozone depletion of 20 to 25% of the total ozone column by late March (Grooß et al., 2004). A major warming associated with a split of the vortex in mid-January stopped the cold phase. Vortex temperatures at the 50 hPa level

[1]Schlager, H., Voigt, C., Volk, M., Davies, S., Carslaw, K., Konopka, P., Roiger, A., and Stock, P.: Observations of denitrification and renitrification in the 2002–2003 Arctic winter stratosphere, Atmos. Chem. Phys. Discuss., in preparation, 2004.

ACPD
4, 8579–8607, 2004

were significantly above T_{NAT} for at least two weeks and NAT particles are not expected to survive this warm period. In early February the vortex gained strength and cooled again. The measurements discussed below were taken under these meteorological conditions on 6 February 2003, before the final warming of the vortex in April.

The Vintersol/Euplex project has the aim to characterize ozone loss and PSCs in the Arctic winter 2002/2003. Within this project, a campaign with the high-altitude research aircraft M55 Geophysica and the Falcon took place from 15 January to 11 February 2003 in Kiruna/Sweden. In this period, the Geophysica performed 10 mission flights to altitudes of 20 km.

3. Instrumentation

The Geophysica carried an NO_y chemiluminescence instrument, a Forward Scattering Spectrometer Probe (FSSP-300), a Microjoule-Lidar and a backscatter sonde for particle detection, besides instruments for trace gas and temperature measurements. Here we concentrate on in-situ measurements of PSCs using the NO_y instrument SIOUX (Schlager et al., in preparation, 2004[1]) and the FSSP (Borrmann et al., 2000).

3.1. NO_y instrument

The NO_y instrument (Schmitt, 2003) is mounted in a pod under the right wing of Geophysica. Here, NO_y is the sum of reactive nitrogen species, of which HNO_3, NO, NO_2, N_2O_5 and $ClONO_2$ are most important in the stratosphere. The inlet of the NO_y instrument is especially designed for PSC particle measurements. Particulate and gas phase NO_y (total NO_y=$NO_{y,tot}$) are measured by a forward facing inlet. Calculations following Krämer and Afchine (2004) show that the measured particle number density is enhanced by a size-dependent factor $E(d)$, which reaches 21 for large particles at 70 hPa. In the rear facing inlet, particles larger than cut-off size d_{50}=0.2 μm are inertially stripped off the sampled air, so that predominantly the gas phase NO_y is measured

ACPD
4, 8579–8607, 2004

(=$NO_{y,gas}$). The heated inlet (35°C) and a subsequent gold converter (300°C) ensure complete evaporation of particulate NO_y and catalytic conversion to NO. Finally the infrared radiation of the reaction NO+O_3 is measured with a chemiluminescence detector. Nitric acid contained in particles is derived by subtracting $NO_{y,gas}$ from $NO_{y,tot}$ and correcting for the particle enhancement (E). The flow through each inlet is controlled at 1 Nlpm (Normal liter per minute). Thus, at a sampling rate of 1 Hz of the instrument, particle number densities $\leq 10^{-4}$ cm^{-3} can be resolved as individual spikes in the total NO_y data. The sensitivity of the instrument is 12 000 counts/ppb NO_y. The accuracy of the NO_y data is ±18% for $NO_{y,tot}$ and ±12% for $NO_{y,gas}$. The detection limit for particulate NO_y is conservatively estimated as 0.3 ppbv (from the difference between the two channels in periods without particle observation when $T > T_{NAT} + 5$ K).

3.2. Optical particle instruments

The forward scattering spectrometer probe (FSSP, Borrmann et al., 2000) measures the radiation scattered by particles which isokinetically fly through the the beam of a HeNe laser in the size range between 0.4 and 23 μm in diameter, divided in 30 channels. Due to ambiguities in the Mie scattering coefficient, the particle number density in the channels between 0.7 and 1.9 μm cannot be resolved. The effective sampling volume of $\sim$10 L min^{-1} resulting from the laser geometry restricts the detection to particles with number densities $n \gtrsim 10^{-4}$ cm^{-3} (with 1 min integration time).

Additionally, two lidars (Adriani et al., 1992; Mitev et al., 2002) onboard the Geophysica were operated to measure the backscatter and depolarisation of particles. The detection limits of the instruments are 3 to 4% in the volume depolarization at 532 nm.

3.3. Rosemount sensor

The temperature has been measured with an accuracy of +0.8/−0.6 K with a Rosemount sensor. Comparisons (M. J. Mahoney, personal communication, 2003) with data from a Microwave Temperature Profiler (MTP) and a PT100 sensor onboard the

Geophysica show that MTP data are on average +0.8 K warmer and the PT100 data are on average −0.1 K colder than Rosemount data.

4. Detection and identification of a NAT PSC

During a flight from Kiruna over the Atlantic on 6 February 2003, HNO_3 containing particles were observed in the stratosphere by the NO_y instrument. Particles were detected during the outbound and the inbound flight leg at similar geographical locations but different altitudes, indicated by red thick lines on the flight track (yellow line) in Fig. 1. On the outbound flight leg, individual spikes in the total NO_y time series (Fig. 2) indicate the presence of particles near 14.65 h universal time (UT) inside the polar vortex at an altitude of 18.3 km (420 K potential temperature). On the inbound flight, particles were detected as enhanced fluctuations in the total NO_y data near 16.35 h UT at an altitude of 19.5 km (440 K potential temperature). The particles were observed at temperatures between 194.5 and 196 K, corresponding to 0.5 to 3.5 K below T_{NAT}. Here T_{NAT} has been calculated following Hanson and Mauersberger (1988) using the gas phase NO_y and the water vapour measurements (Schiller et al., 2002) onboard the Geophysica.

Under these stratospheric conditions, NAT is the only nitrogen-containing condensed phase known to be stable. The metastable nitric acid dihydrate (NAD) (Worsnop et al., 1993) can only form at $T \leq T_{NAT} - 2.3$ K. Significant uptake of nitric acid in STS droplets starts 3.5 K below T_{NAT} and the resulting particle number densities of 10 cm^{-3} could not produce isolated peaks in the NO_y data. Therefore we assume that the measured particles consist of NAT.

4.1. NAT particle number density and size distribution

We derive particle sizes for the individual peaks in the total NO_y data ascribing them to NAT. Modifying an equation from Northway et al. (2002), the particle diameter is:

$$D[\mu m] = 4.67 \times (\Delta NO_y[ppbv]/0.9)^{0.33} \quad (1)$$

ACPD
4, 8579–8607, 2004

This assumes 90% of the signal of a NAT particle to be captured during the measurement interval of 1 s, as suggested by the instrument response function. Spikes in the Δ NO_y between 0.6 and 1.3 ppbv (see Fig. 2c) correspond to NAT particles with diameters d=4.1–5.4 μm. These particles have a number density $n \sim 6 \times 10^{-6}$ cm^{-3}, derived using the sampling flow and the particle enhancement factor $E(d)$.

In addition, enhanced fluctuations in the ΔNO_y signal (Fig. 2c and d) indicate the presence of smaller particles with higher number densities ($n \geq 10^{-4}$ cm^{-3}), but these cannot be resolved individually. Therefore, we derive the particle number density and size distribution using forward Monte Carlo simulations of the occurrence histogram of the ΔNO_y data. For the simulations, we make an initial guess of the particle size distribution, which consists of a mode of NAT particles and a second mode of smaller STS particles, which have slightly grown due to HNO_3 uptake. We account for oversampling $E(d)$ and assume that the particles evaporate instantly. Further we consider the response time of the instrument, determined by the pumping speed and the volumes of the conversion chamber and the detection chamber. In addition, the instrument noise has been determined from the data between 14.8 and 15.5 h (UT). We add the simulated ΔNO_y signals stochastically and compare the simulated occurrence histogram with the histogram measured in the cloud between 14.55 and 14.75 h (UT). If the agreement is not sufficient, we redefine the size distribution and repeat the steps detailed above.

Good agreement between the measured occurrence histogram of the ΔNO_y data and the simulations (Fig. 3a) is achieved for NAT particles with diameters between 2 and 5.4 μm at number densities of 1.6×10^{-4} cm^{-3} (thick black line in Fig. 3b). NAT particles with diameters <2 μm cannot be resolved from the data as their signal is masked in slightly enhanced ternary background aerosol containing ~0.03 ppbv HNO_3 (curved thick black line in Fig. 3b). Sensitivity studies indicate that both doubling or halving the NAT particle number density (thin black solid and dashed lines in Fig. 3a) leads to significant deteriorations of the fit. A similar analysis (not shown here) has been performed for the NAT particles detected on the return flight leg at 19.5 km altitude just

ACPD
4, 8579–8607, 2004

above the region of particle detection at 18.3 km (Fig. 2d). Those ΔNO_y data can be simulated using NAT particles with diameters between 1 and 3.5 μm at a number density of 3×10^{-4} cm^{-3} superimposed to ternary solution aerosols containing ~0.04 ppbv nitric acid. The error in the NAT particle number density derived from the simulations is ± a factor of 2.

We now compare the particle size distribution derived from the simulations to the measurements of the optical instruments. The depolarisation produced by 10^{-4} cm^{-3} NAT particles with diameters smaller than 5 μm is less than 1.5% in the volume depolarisation, therefore it lies below the detection limit of 3 to 4% of the two lidars. Conversely, the FSSP detected 3 particles with diameters d=1.9–4.6 μm near 14.65 h UT at 18.3 km altitude besides a small background aerosol mode (thin black line with error bars in Fig. 3b). Thus, we use the FSSP data as additional support for the particle size distribution derived from the NO_y instrument, but the low sampling statistics does not allow for a more precise data comparison. In summary, there is an agreement between the particle size distributions derived from the optical particle instruments and the NO_y instrument.

4.2. Extension and vertical structure of the NAT cloud

On 6 February 2003, a NAT PSC is measured inside the polar vortex above the Atlantic ocean near the Norwegian coast (red lines in Fig. 1). At an altitude of 18.3 km (420 K), a low number density cloud (n~1.6×10^{-4} cm^{-3}) of NAT particles with d<6 μm are detected over a distance of 140 km. Above these particles, almost twice the number density of smaller NAT particles (d<3.5 μm) are measured at 19.5 km (440 K) over a distance of 250 km, probably in the same cloud. The upward and downward looking micro-lidar (Mitev et al., 2002) onboard the Geophysica measures no significant increase of depolarisation and backscatter ratios at 532 nm above the background aerosol level in the region 5 km above and below the flight track in the stratosphere. Thus, the NAT particles were measured in an optically thin NAT cloud.

ACPD
4, 8579–8607, 2004

4.3. Simulations of the NAT PSC

We calculated how large a NAT particle can grow at different temperatures assuming 5 ppmv water and 10 ppbv nitric acid in the gas phase and taking into account the uptake of nitric acid into STS aerosol (Fig. 4). A NAT particle grows to a diameter of 6 μm, if temperatures remain 2 K below T_{NAT} for 16 h. When temperatures reach the ice frost point, the NAT particle growth is reduced due to nitric acid gas phase depletion by HNO_3 uptake into ternary solution particles. The slower growth of the particles to the same size at these extremely low temperatures reflects the fact that it takes time to release the HNO_3 from the metastable STS droplets, to establish its diffusive transport through the gas phase and finally its uptake by the NAT particle in a Bergeron-Findeisen-like process.

Further we performed a vortex wide simulation of NAT particles using the DLAPSE model, which couples a Lagrangian NAT particle growth and sedimentation scheme to the three-dimensional (3-D) chemistry transport model SLIMCAT (Carslaw et al., 2002). To adequately reproduce denitrification measured in the Arctic winter 2002/2003 (Schlager et al., in preparation, 2004[1]) we increase the NAT nucleation rate by a factor of 4 (Davies et al., 2004) compared to the run for the 1999/2000 winter (Mann et al., 2003). We further increase the number of explicitly calculated model particles by a factor of 10 and in turn reduce the model scaling factor by a factor of 10 to improve the statistics for low particle number densities. The existence of 1.5×10^{-4} cm^{-3} NAT particles with d=1–7 μm is calculated with the DLAPSE model near the flight track on 6 February 2003 in good agreement with the observations. Figure 3b (dashed line) shows the modeled NAT particle size distribution in a region of 66–69° latitude north and 12–16° longitude east at 410 to 430 K potential temperature. At higher altitudes between 430 and 450 K, the existence of smaller NAT particles with a higher number density is simulated with the DLAPSE model in qualtiative agreement with the observations.

We note that the DLAPSE model simulates NAT particles in a slightly larger area than

ACPD
4, 8579–8607, 2004

observed (red line in Fig. 1) and also the shape of the size distributions differs from the observations. This may result from the simulation of NAT formation at a constant rate at temperatures below T_{NAT}. In the real atmosphere, the particle nucleation process depends on temperature, NAT supersaturation and variations of the air masses. Assuming an increase in the NAT nucleation rate with NAT supersaturation could explain those discrepancies in the shape of the size distribution and the region of particle observation.

4.4. Comparison with other PSC measurements

Between 15 January and 11 February 2003, in total 10 flights have been performed with the Geophysica during the Euplex campaign. The excellent performance of the particle channel of the NO_y instrument was demonstrated by several cirrus cloud encounters. Thin liquid ternary solution PSCs containing up to 0.5 ppbv nitric acid have been detected in mountain waves in two flights (Lowe et al., in preparation, 2004[2]). Temperatures below T_{NAT} were encountered on 4 flights. In all those cases, the trajectory temperatures were below T_{NAT} for less than 8 h except for 6 February. In 8 h, a NAT particle can grow to a size of 3.3 μm in diameter and contains ~0.3 ppbv NO_y, which is near the PSC particle detection limit of the NO_y instrument. Except for cirrus clouds, nitric acid containing particles with diameters larger than 3.3 μm have only been detected on 6 February 2003.

We now compare the PSC measured on 6 February 2003 with other PSC observations. In winter 1999/2000, NO_y containing particles with larger diameters between 10 and 20 μm and $n \sim 10^{-4}$ cm^{-3} have been detected (Fahey et al., 2001; Northway et al., 2002). These particles could also be inferred from extinction data of satellite measurements (Poole et al., 2003). In addition, NAT particles with median diameters around

[2]Lowe, D., MacKenzie, A. R., Schlager, H., et al.: Liquid particle composition and heterogeneous reactions in a liquid polar stratospheric cloud, Atmos. Chem. Phys. Discuss., in preparation, 2004.

ACPD
4, 8579–8607, 2004

3 μm and number densities of a few times 10^{-3} cm^{-3} have been detected during several balloon flights in Arctic mountain waves (Deshler et al., 2003; Schreiner et al., 2003) or during synoptic cooling (Larsen et al., 2004). Fahey et al. (2001) also mention a second smaller particle mode with diameters between 3 and 4 μm and $n \sim 10^{-3}$ cm^{-3} without giving more details. Measurements of low number densities ($n \sim 10^{-4}$ cm^{-3}) of small NAT particles ($d < 6\,\mu$m) as observed in the present case have not been reported so far.

5. Trajectory analysis

The particle measurements on 6 February 2003 took place in a short period with temperatures for a few days slightly below T_{NAT} in the lower Arctic stratosphere. Therefore we performed an accurate trajectory analysis to gain new insights in PSC formation at threshold PSC formation conditions.

We calculated trajectories based on ECMWF analysis ending in a wider region around the flight track indicated by the white square in Fig. 1. The backtrajectories were started on a grid in steps of 0.5° in latitude and longitude and at altitudes of 70 hPa (pressure altitude on the outbound flight leg), 55 hPa (pressure altitude on the return flight leg) and 50 hPa. The difference between the trajectory temperatures at 70 hPa and T_{NAT}, calculated based on the measured NO_y and water profile, is shown in Fig. 5. Those trajectories ending in regions with NAT particles observations are marked by red lines in Fig. 5. In the time period of one day, the descent rate of particles with diameters $< 5\,\mu$m due to gravitational settling is slow ($\leq$200 m/day) and comparable to the descent rate air by diabatic cooling ($\sim$100 m/day). Therefore, we consider the calculated air parcel temperature as an approximated temperature history of the NAT particles.

The trajectory temperatures were above T_{NAT} for at least 9 days before they decrease below T_{NAT} approximately 20 h before the particle detection. The absolute temperature minimum reached by any of the trajectories is $T \sim T_{NAT} - 3.5$ K or $T \sim T_{ice} + 4$ K. This con-

clusion holds even when allowing for mesoscale temperature fluctuations related to gravity waves above the Scandinavian Alps (orange lines in Fig. 4), which we calculated using the MM-5 mesoscale model (Dörnbrack et al., 1999). For the return flight leg at 55 hPa and also at the 50 hPa level, the trajectory temperatures (not shown here) were even higher. They were less than 19 h below T_{NAT} reaching minimum values of $T_{NAT}-2.4$ K. This meteorological situation with low atmospheric temperature variability allows us to constrain temperatures for particle formation to $T>T_{NAT}-3.5$ K corresponding to NAT saturation ratios $S_{NAT}\lesssim 11$.

6. NAT formation

Given that the trajectory temperatures remain 20 h below T_{NAT}, we can derive an average NAT nucleation rate of $J_{NAT}=8\times10^{-6}$ cm^{-3} air h^{-1} at temperatures below T_{NAT} to explain the measured particle number density of 1.6×10^{-4} cm^{-3}. A slightly lower NAT nucleation rate has been determined for the winter 1999/2000 (3×10^{-6} cm^{-3} air h^{-1}) (Fahey et al., 2001; Carslaw et al., 2002). Different studies exist for the winter 2002/2003. A higher NAT nucleation rate (2.5×10^{-5} cm^{-3} air h^{-1}) has been derived from balloon-borne measurements of NAT particle number densities at lower temperatures (Larsen et al., 2004) in December 2002. The denitrification in the Arctic winter 2002/2003 can well be modeled using a nucleation rate of $J_{NAT}=1.15\times10^{-5}$ cm^{-3} air h^{-1} (Davies et al., 2004; Schlager et al., in preparation, 2004[1]). Grooß et al. (2004) investigate the effect of different nucleation rates on the denitrification.

NAT nucleation is a subject of current scientific debate (Tolbert and Toon, 2001). Here we use the NAT cloud observation in this unique situation at threshold NAT formation conditions ($S_{NAT}\lesssim 11$) to discuss different theories of NAT particle formation.

ACPD
4, 8579–8607, 2004

6.1. Homogeneous NAT nucleation

Homogeneous nucleation rates of NAT/NAD in ternary solutions have been determined from laboratory experiments (Koop et al., 1995, 1997; Salcedo et al., 2001; Knopf et al., 2002). Other laboratory studies with binary solutions show that the metastable NAD may form as the precursor of NAT, later performing a transition to NAT (Worsnop et al., 1993). The results of our trajectors analysis ($T > T_{NAT} - 3.5$ K) strongly suggest, that those particle are neither composed of NAD nor have nucleated on NAD. Another analysis of laboratory experiments suggests that the nucleation of solids occurs on the surface rather than in the volume of liquid particles (Tabazadeh et al., 2002). At temperatures above $T_{NAT} - 3.5$ K or NAT saturation ratios $S_{NAT} \lesssim 11$, the nucleation rates given in each of those laboratory studies cited above are by 1 to 8 orders of magnitude too low to explain the present observations.

6.2. NAT sedimentation from higher altitudes

The air parcels have been exposed to temperatures at least 7 K above T_{NAT} during the 9 days before decreasing below T_{NAT} approximately one day before the measurements (Fig. 5). Above the observational levels at 50 hPa the trajectory temperatures take a similar course, first too warm for NAT and cooling only on the day of the observation. A 16 μm NAT particle evaporates within 8 h at 3 K above T_{NAT}. Therefore previously formed NAT particles would not survive such a warm period and the air must be NAT free on 5 February 2003. Thus the measured NAT particles have formed in less than a day. In one day, a NAT particle can grow to a maximum diameter of 8 μm and sediment less than 500 m, therefore sedimentation of NAT particles from higher altitudes is negligible.

Additionally, the dynamical activity in the stratosphere due to mesoscale wave activity is low on 6 February with maximum temperature deviations of the mesoscale trajectories of ±0.7 K from ECMWF trajectories (Fig. 4). Further, the minimum trajectory temperatures of $T_{NAT} - 3.5$ K are reached above the Atlantic ocean, where the effect

of mesoscale wave activity is small. In addition, the upward looking lidar onboard the Geophysica did not detect a mountain wave PSC. Summarized NAT sedimentation out of mountain wave clouds (Carslaw et al., 1999; Dhaniyala et al., 2002; Füglistaler et al., 2002) can be ruled out.

6.3. Heterogeneous NAT nucleation on ice

Lidar and in situ measurements in mountain wave PSCs (Carslaw et al., 1998; Wirth et al., 1999; Voigt et al., 2000a) as well as model simulations (Luo et al., 2003) show that NAT can nucleate on ice. However, on 6 February 2003 NAT nucleation on ice can be excluded, because the synoptic ECMWF trajectories and even the mesoscale MM5 trajectories were by more than 4 K above the T_{ICE}, thus significantly too high for ice formation. The present measurements convincingly demand a NAT formation mechanism above the ice frost point, which has also been claimed in recent model studies (Carslaw et al., 2002; Drdla et al., 2003) or PSC observations (Larsen et al., 2004). Conversely to the present case, the PSC trajectories in the study of Larsen et al. (2004) almost reach the ice frost point or NAT saturation ratios S_{NAT}~30.

6.4. NAT nucleation on meteoritic particles

Obviously potent nuclei must be available with sufficiently low surface areas, on which NAT can nucleate either by heterogeneous immersion nucleation (when the nuclei are immersed in the preexisting STS droplets) or by heterogeneous deposition nucleation (directly via nucleation of NAT from the gas phase). One potentially important, ubiquitous kind of nuclei are meteoritic smoke particles. Most (60 %) of the meteoritic mass influx in the atmosphere of 16×10^6 kg per year (best estimate, 8–30×10^6 kg yr^{-1}) ablates at altitudes above 75 km due to frictional heating in the atmosphere (Cziczo et al., 2001). Model studies indicate that the ablation products recondense and coagulate in the mesosphere forming nanometer-sized smoke particles (Hunten et al., 1980). Following atmospheric circulation and sedimentation, most of the meteoritic particles

ACPD
4, 8579–8607, 2004

are likely to enter the stratosphere over the winter pole. The meteoritic particles traverse the stratosphere in more than a year, during which they may become well-mixed, homogenized and partly incorporated into the stratospheric sulfate aerosol (Cziczo et al., 2001). Mass spectrometric measurements detected meteoritic inclusions in half of the stratospheric particles (Murphy et al, 1998; Cziczo et al., 2001). Curtius et al. (in preparation, 2004)[3] report in a detailed study that the fraction of stratospheric particles containing detectable amounts of involatile material (probably of meteoritic origin) increases markedly inside the polar vortex to ∼70%.

We estimate the meteoritic surface area by assuming that 50% of the stratospheric sulfate aerosol with a typical lognormal size distribution (d_m=0.15 μm, σ=1.65, n=10 cm^{-3}) (Fig. 3) (Deshler et al., 2003) and a density of 1.72 g cm^{-3} (72 wt% sulfuric acid/water solution) contains 0.75 wt% meteoritic iron (Cziczo et al., 2001). Further we assume that meteoritic material with a density of 3 g cm^{-3} contains 20 wt% meteoritic iron (Cziczo et al., 2001). Then we derive a meteoritic surface area density A_{min}=0.05 μm^2 cm^{-3} using the Hatch-Chaote-Equation (Hinds, 1999) for 2.4 vol% meteoritic inclusions (with a mean diameter d_m=0.044 μm) in 50% of the stratospheric sulfate particles. Model simulations of continuously coagulating spherical meteoritic smoke particles derive a meteoritic surface area density of similar magnitude (A∼0.1 μm^2 cm^{-3}, Hunten et al., 1980). The meteoritic surface area may be underestimated by up to two orders of magnitude, because the meteoritic smoke particles are expected to form loosely packed agglomerations and not spheres, i.e. A=0.05–5.0 μm^2 cm^{-3} (Cziczo et al., 2001; Hunten et al., 1980). Additionally, variations in the extraterrestrial meteoritic flux or seasonal/interannual changes in the stratospheric circulation, including the formation of the polar vortex, can lead to inhomogeneities and variations of the meteoritic surface area.

Heterogeneous nucleation of ternary solutions on micro-meteorites has been inves-

[3]Curtius, J., Weigel, R., Vössing, H.-J., et al.: In-situ particle measurements in the winter Arctic lower stratosphere: Implications for particle nucleation and volatility, Atmos. Chem. Phys. Discuss., in preparation, 2004.

tigated calorimetrically. Biermann et al. (1996) found that the presence of meteoritic material accelerates the freezing of supercooled ternary solutions. They determined an upper limit of the heterogeneous NAT nucleation rate per surface area of meteoritic material of $j_{max}=1.4\times10^{-4}\mu m^{-2}$ h^{-1} at $S_{NAT}\sim20$ (their measurements referring to "solution 2").

By combining the laboratory data and in situ measurements of meteoritic particles, we obtain a very rough estimate for the NAT nucleation rate on meteoritic particles of $J_{NAT}=j_{max}\times A_{min}=7\times10^{-6}$ cm^{-3} h^{-1} in the stratosphere. Although this neatly coincides with the experimentally observed value $J_{NAT}=8\times10^{-6}$ cm^{-3} air h^{-1}, we note that an estimate based on a product of an upper and a lower limit (for the rate and for the surface area, respectively) needs to be treated with caution. Since the heterogeneous nucleation of NAT has not been investigated at NAT saturation ratios as low as observed on 6 February, $S_{NAT}<11$, there is an additional gulf of uncertainty in this result. Conversely, the investigation of Biermann and coworkers refers only to immersion nucleation, while deposition nucleation remains another possible and yet untested pathway for NAT nucleation.

Given the present knowledge, NAT nucleation on ubiquitous meteoritic particles must be regarded as a possible pathway for the formation of solid polar stratospheric cloud particles at low number densities. Assuming temperatures below T_{NAT} for 3 days (instead of 1 day as during EUPLEX), the estimated rate can produce NAT particle number densities up to few times 10^{-4} cm^{-3}, thus might explain the observations by Fahey et al. (2001).

In summary, contrasting to the conclusions of Biermann et al. (1996), who aimed at excluding meteoritic material as responsible for dense ($n>10^{-2}$ cm^{-3}) NAT clouds, the discovery of large singular NAT particles ("NAT rocks", $n\sim10^{-4}$ cm^{-3}) makes meteoritic smoke particles favorable candidates for triggering NAT nucleation.

ACPD
4, 8579–8607, 2004

6.5. Effective NAT nucleation rate

In classical nucleation theory, the nucleation rate strongly depends on the NAT saturation ratio, $J \sim \exp(-A(T)/(\ln S_{NAT})^2)$, where A is a function of temperature. If we assume such a dependency, the nucleation process acts like a switch and all available nuclei may be activated within a small temperature range, which is contradictory to the variety of PSC number densities observed in the winter 2002/2003 or in previous winters. To consistently model the existing PSC observations, either more than one type of nucleus or different nucleation mechanisms may be required, which is conceivably true for meteoritic material. All those processes may add up, smearing the dependency on S_{NAT} and resulting in an average effective NAT nucleation rate.

7. Conclusions

Low number densities ($n \sim 1.6 \times 10^{-4}\,\mathrm{cm}^{-3}$) of NAT particles with diameters $d < 6\,\mu\mathrm{m}$ have been detected by in-situ instruments onboard the Geophysica in the Arctic polar stratosphere in winter 2002/2003. In contrast to previous observations, those particles have formed in less than a day at high temperatures ($T > T_{NAT} - 3.5\,\mathrm{K}$) thus very low NAT supersaturations ($S_{NAT} \lesssim 11$), which until recently has not been considered likely to happen. NAT nucleation at temperatures so close to T_{NAT} increases the time scales and regions of PSC occurrence, which in turn may lead to more efficient denitrification and thus to enhanced polar ozone loss.

Given the scarcity of data, we estimate here a constant average NAT nucleation rate $J_{NAT} = 8 \times 10^{-6}\,\mathrm{cm}^{-3}\,\mathrm{air\,h}^{-1}$ for the temperature range $T_{NAT} > T > T_{NAT} - 3.5\,\mathrm{K}$. A dependence on temperature or NAT supersaturation can not be determined from these data. Also, the NAT nucleation rate may vary from year to year or during the course of a winter. For the late Arctic winter 2002/2003 calculations with the effective nucleation rate of $8 \times 10^{-6}\,\mathrm{cm}^{-3}\,\mathrm{air\,h}^{-1}$ as derived in the present study reasonably reproduce our observations of NAT particle number density, size distribution and additionally of

ACPD
4, 8579–8607, 2004

denitrification measured by SIOUX (Schlager et al., in preparation, 2004[1]) or satellite (Davies et al., submitted, 2004).

We show that NAT nucleation on ubiquitous meteoritic smoke particles may present a pathway for solid particle formation at temperatures above the ice frost point. However, the detailed mechanism and the spatial and temporal variation of the meteoritic smoke particles as well as the temperature dependence of the NAT nucleation rate on these remain a challenge for future laboratory and field studies.

Acknowledgements. We thank the Geophysica crew, F. Stroh for excellent project coordination, J.-U. Grooß for trajectory data, M. Mahoney for temperature comparisons, R. Weigel for CN counter data, F. Cairo and R. Matthey for data from optical instruments, K. Carslaw and M. Krämer for helpful discussions. We thank the European Centre for Medium-range Weather Forecasts and MeteoSwiss for meteorological data. This work has been funded by the European Community and the Swiss BBW under the contracts EVK2-2001-00084-EuPLEx and EVK-2000-00077-MAPSCORE.

References

Adriani, A., Deshler, T., Gobbi, G. P., et al.: Polar stratospheric clouds over McMurdo, Antarctica, during the 1991 spring: Lidar and particle counter measurements, Geophys. Res. Lett., 19(17), 1755–1758, doi:10.1029/92GL01941, 1992.

Biermann, U. M., Presper, T., Koop, T., et al.: The Unsuitability of Meteoritic and Other Nuclei for Polar Stratospheric Cloud Freezing, Geophys. Res. Lett., 23, 1693–1696, 1996.

Borrmann, S., Thomas, A., Rudakov, V., et al.: In-situ aerosol measurements in the northern hemispheric stratosphere of the 1996/7 winter on the Russian M-55 Geophysika high altitude research aircraft, Tellus, 52B, 1088–1103, 2000.

Carslaw, K. S., Luo, B. P., Clegg, S., et al.: Stratospheric aerosol growth and HNO_3 gas phase depletion from coupled HNO_3 and water uptake by liquid particles, Geophys. Res. Lett., 21, 2479–2482, 1994.

Carslaw, K. S., Wirth, M., Tsias, A., et al.: Particle Microphysics and Chemistry in Remotely Observed Mountain Polar Stratospheric Clouds, J. Geophys. Res., 103, 5785–5796, 1998.

Carslaw, K. S., Peter, T., and Bacmeister, J. T.: Widespread solid particle formation by mountain waves in the Arctic stratosphere, J. Geophys. Res., 104(D1), 1827–1836, doi:10.1029/1998JD100033, 1999.
Carslaw, K. S., Kettleborough, J. A., Northway, M. J., et al.: A vortex-scale simulation of the growth and sedimentation of large nitric acid hydrate particles, J. Geophys. Res., 107 (D20), 8300, doi:10.1029/2001JD000467, 2002.
Cziczo, D. J., Thomson, D. S., and Murphy, D. M.: Ablation, Flux and Atmospheric Impications Inferred from Stratospheric Aerosol, Science, 291, 1772–1775, 2001.
Davies, S., Mann, G., Carslaw, K. S., et al.: 3-D microphysical model studies of Arctic denitrification: comparison with observations, Atmos. Chem. Phys. Discuss., accepted, 2004.
Deshler, T., Larsen, N., Weisser, C., et al.: Large nitric acid particles at the top of an Arctic stratospheric cloud, J. Geophys. Res., 108 (D16), 4517, doi:10.1029/2003JD003479, 2003.
Dörnbrack, A., Leutbecher, M., Kivi, R., and Kyrö, E.: Mountain-wave induced record low stratospheric temperatures above northern Scandinavia, Tellus, 51A, 951–963, 1999.
Drdla, K., Schoeberl, M. R., and Browell, E. V.: J. Geophys. Res., 108 (D5), 8312, doi:10.1029/2001JD000782, 2003.
Dhaniyala, S., McKinney, K. A., and Wennberg, P. O.: Lee-wave clouds and denitrification of the polar stratosphere, Geophys. Res. Lett., 29 (9), doi:10.1029/2001GL013900, 2002.
Fahey, D., Solomon, S., Kawa, S. R., et al.: Observations of denitrification and dehydration in the polar winter stratosphere, Nature, 344, 321–324, 1990.
Fahey, D. W., Gao, R. S., Carslaw, K. S., et al.: The detection of large HNO_3-containing particles in the winter arctic stratosphere, Science, 291, 1026–1031, 2001.
Fueglistaler, S., Luo, B. P., Voigt, C., et al.: NAT-rock formation by mother clouds: a microphysical model study, Atmos. Chem. Phys., 2, 93–98, 2002.
Grooß, J. U., Günther, G., Müller, R., et al.: Simulation of denitrification and ozone losse for the Arctic winter 2002/2003, Atmos. Chem. Phys. Discuss., 4, 8069–8101, 2004.
Hanson, D. and Mauersberger, K.: Laboratory studies of the nitric acid trihydrate: Implications for the south polar stratosphere, Geophys. Res. Lett., 15, 855–858, 1988.
Hinds, W. C.: Aerosol technology: properties, behaviour, and measurement of airborne particles, 2nd ed., John Wiley & Sons, Inc., New York, 1999.
Hunten, D., Turco, R. P., and Toon, O. B.: Smoke and Dust Particles of Meteoric Origin in the Mesosphere and Stratosphere, J. Atmos. Sci., 37, 6, 1342–1357, 1980.
Knopf, D. A., Koop, T., Luo, B. P., et al.: Homogeneous nucleation of NAD and NAT in liquid

stratospheric aerosols: insufficient to explain denitrification, Atmos. Chem. Phys., 2, 207–214, 2002.
Koop, T., Biermann, U. M., Raber, W., et al.: Do stratospheric aerosol droplets freeze above the ice frost point?, Geophys. Res. Lett., 22(8), 917–920, doi:10.1029/95GL00814, 1995.
Koop, T., Luo, B. P., Biermann, U., et al.: Freezing of $HNO_3/H_2SO_4/H_2O$ Solutions at Stratospheric Temperatures: Nucleation Statistics and Experiments, J. Phys. Chem. A, 101, 1117–1133, 1997.
Koop, T., Luo, B. P., Tsias, A., and Peter, T.: Water activity as the determinant for homogeneous ice nucleation in aqueous solutions, Nature, 406, 611–614, 2000.
Krämer, M. and Afchine, A.: Sampling characteristics of inlets operated at low U/U_0 ratios: new insights from computational fluid dynamics (CFX) modeling, J. Aerosol Sci., 35, 6, 683–694, 2004.
Larsen, N., Knudsen, B., Svendsen, S., et al.: Formation of solid particles in synoptic-scale Arctic PSCs in early winter 2002/2003, Atmos. Chem. Phys., 4, 2001–2013, 2004.
Luo, B., Voigt, C., Füglistaler, S., and Peter, T.: Extreme NAT supersaturations in mountain wave ice PSCs: a clue to NAT formation, J. Geophys. Res., 108 (D15), 4441, doi:10.1029/2002JD003104, 2003.
Mann, G., Davies, S., Carslaw, K., and Chipperfield, M.: Factors controlling Arctic denitrification in cold winters of the 1990s, Atmos. Chem. Phys., 3, 403–416, 2003.
Mitev, V., Matthey, R., and Makarov, V.: Miniature backscatter lidar for cloud and aerosol observation from high altitude aircraft, Rec. Res. Devel. Geophys., 4, 207, ISBN: 81-7736-076-0, 2002.
Murphy, D. M., Thomson, D. S., and Mahoney, M. J.: In situ Measurements of Organics, Meteoritic Material, Mercury and Other Elements in Aerosols at 5 to 19 Kilometers, Science, 282, 1664–1667, 1998.
Northway, M. J., Gao, R. S., Popp, P. J., et al.: An analysis of large HNO_3-containing particles sampled in the Arctic stratosphere during the winter of 1999–2000, J. Geophys. Res., 107, 8289, doi:10.1029/2001JD001079, 2002.
Peter, T.: Microphysics and heterogeneous chemistry of polar stratospheric clouds, Ann. Rev. Phys. Chem., 48, 785–822, 1997.
Poole, L. R., Trepte, C. R., Harvey, V. L., et al.: SAGE III observations of Arctic polar stratospheric clouds – December 2002, Geophys. Res. Lett., 30, 23, 2216–2220, 2003.
Salcedo, D., Molina, L. T., and Molina, M. J.: Homogeneous Freezing of Concentrated Aqueous

Nitric Acid Solutions at Polar Stratospheric Temperatures, J. Phys. Chem., 105, 1433–1439, 2001.
Schreiner, J., Voigt, C., Kohlmann, A., et al.: Chemical analysis of polar stratospheric cloud particles, Science, 283, 968–970, 1999.
Schreiner, J., Voigt, C., Mauersberger, K., et al.: Chemical, microphysical, and optical properties of polar stratospheric clouds, J. Geophys. Res., 108, 8313, doi:10.1029/2001JD000825, 2003.
Schiller, C., Bauer, R., Cairo, F., et al.: Dehydration in the Arctic stratosphere during the SOLVE/THESEO-2000 campaigns, J. Geophys. Res., 107 (D20), 8293, doi:10.1029/2001JD000463, 2002.
Schmitt, J.: Aufbau und Erprobung eines in-situ NO/NOy-Mess-Systems am Höhenforschungsflugzeug Geophysica, PhD Thesis, edited by: DLR, D-51170 Köln, ISRN DLR-FB-2003-21, 2004.
Scientific Assessment of ozone depletion, 1998, WMO Report No. 44, Geneva, 1999.
Tabazadeh, A., Djikaev, Y. S., Hamill, P., et al.: Laboratory evidence for surface nucleation of Solid Polar Stratospheric Cloud Particles, J. Phys. Chem. A, 106, 10 238–10 246, 2002.
Thomas, A.: In situ measurements of background aerosol and subvisible cirrus in the tropical tropopause region, J. Geophys. Res., 107 (D24), 4763, doi:10.1029/2001JD001385, 2002.
Tolbert, M. and Toon, B.: Solving the PSC mystery, Science, 292, 61–63, 2001.
Toon, O. B., Tabazadeh, A., Browell, E. V., and Jordan, J.: Analysis of lidar observations of Arctic polar stratospheric clouds during January 1989, J. Geophys. Res., 105(16), 20 589–20 615, 2000.
Voigt, C., Schreiner, J., Kohlmann, A., et al.: Nitric Acid Trihydrate (NAT) in Polar Stratospheric Clouds: Science, 290, 1756–1758, 2000a.
Voigt, C., Tsias, S., Dörnbrack, A., et al.: Non-equilibrium compositions of liquid polar stratospheric clouds in gravity waves, Geophys. Res. Lett., 27, 3873–3876, 2000b.
Voigt, C., Larsen, N., Deshler, T., et al.: In situ mountain-wave polar stratospheric cloud measurements: Implications for nitric acid trihydrate formation, J. Geophys. Res., 108, D5, doi:10.1029/2001JD001185, 2003.
Waibel, A., Peter, T., Carslaw, K. S., et al.: Arctic Ozone Loss Due to Denitrification, Science, 283, 2064–2069, 1999.
Wirth, V., Tsias, A., Dörnbrack, A., Weiß, V., Carslaw, K. S., Leutbecher, M., Renger, W., Volkert, H., and Peter, T.: Model-guided Lagrangian observation and simulation

of mountain polar stratospheric clouds, J. Geophys. Res., 104(D19), 23 971–23 982, doi:10.1029/1998JD900095, 1999.
Worsnop, D. R., Fox, L. E., Zahniser, M. S., and Wofsy, S. C.: Vapor pressures of solid hydrates of nitric acid: implications for polar stratospheric clouds, Science, 259, 71–74, 1993.

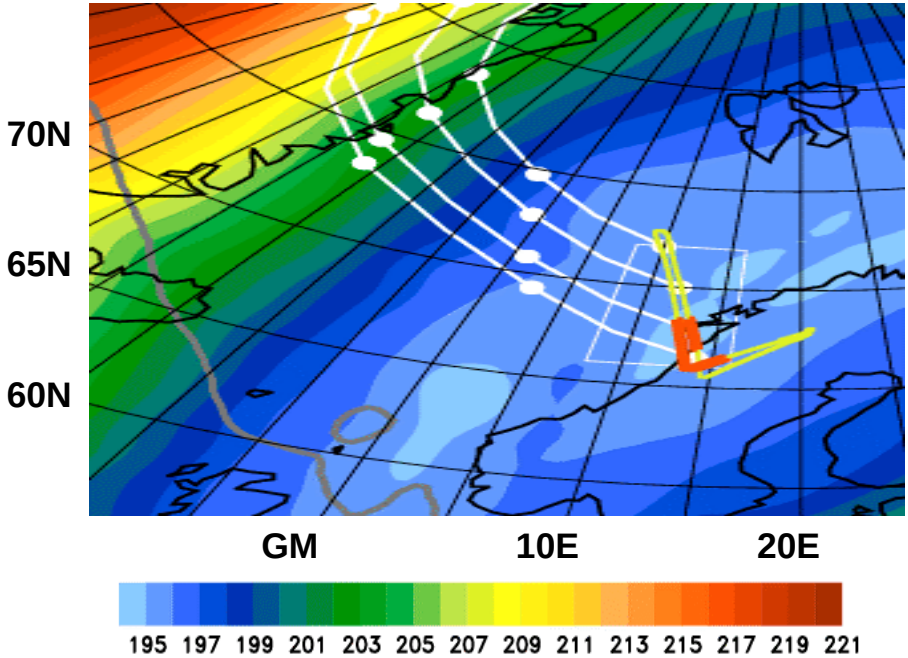

Fig. 1. ECMWF analysed temperature (K, color coded) at 60 hPa on 6 February 2003 at 12:00 UT. The flight path is marked in yellow and the part of the flight with particle observations is marked by the thick red line. White lines indicate selected air parcel backward trajectories. Each white dot marks a duration of 12 h. The white square indicates the region, in which the parcel trajectories end. The thick grey line is the vortex edge, defined by a potential vorticity of 3×10^{-6} km^2 kg^{-1} s^{-1}.

ACPD
4, 8579–8607, 2004

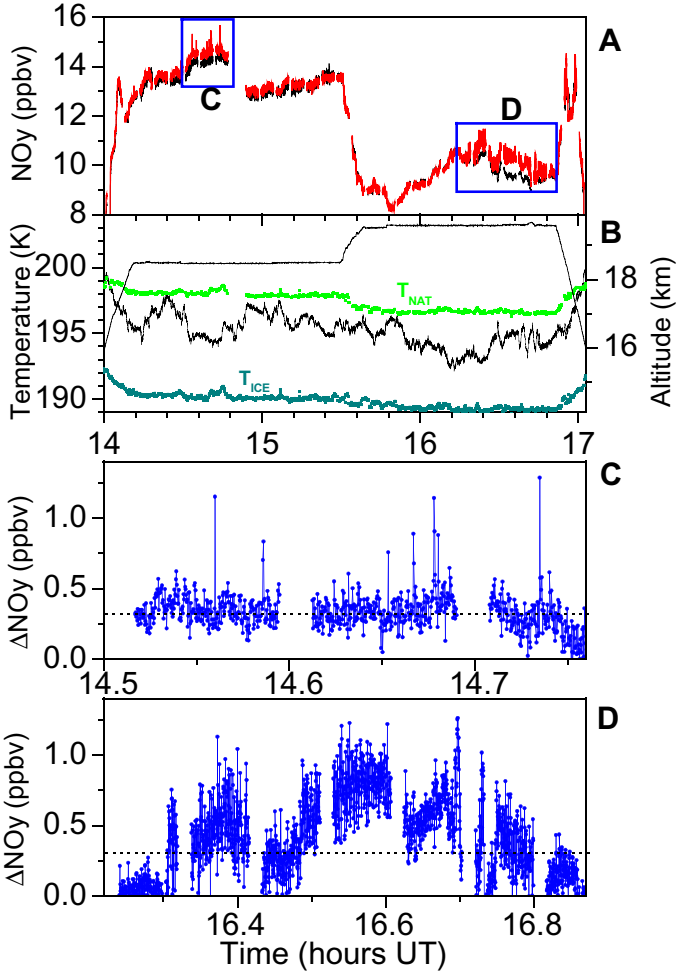

Fig. 2.

ACPD
4, 8579–8607, 2004

Nitric acid trihydrate (NAT) formation at low NAT supersaturations

C. Voigt et al.

(A) Total NO_y (gas phase plus enhanced particulate NO_y) measurements through the forward facing inlet (red curve) and gas phase NO_y measurements through the backward facing inlet (black curve) versus universal time (UT) on 6 February 2003. Regions with particle observations (red flight segments in Fig. 1) are marked by blue squares. **(B)** Flight altitude (grey), temperature (black), T_{NAT} (green dots) and T_{ICE} (cyan dots). T_{NAT} and T_{ICE} have been calculated using gas phase NO_y measurements and water vapor measurements onboard the Geophysica. The particles have been observed at $T>T_{ICE}+4$ K. **(C, D)** Expanded view of particulate reactive nitrogen, ΔNO_y, in regions marked by blue squares in (A). ΔNO_y derives from a subtraction of $NO_{y,tot}$ and $NO_{y,gas}$. Note that ΔNO_y has to be corrected for particle enhancement, $E(d)$. Particles are indicated by individual peaks in the data (C) and by intensified signal fluctuations (C and D). The dashed black line in (C and D) shows the detection limit for particle NO_y.

ACPD

4, 8579–8607, 2004

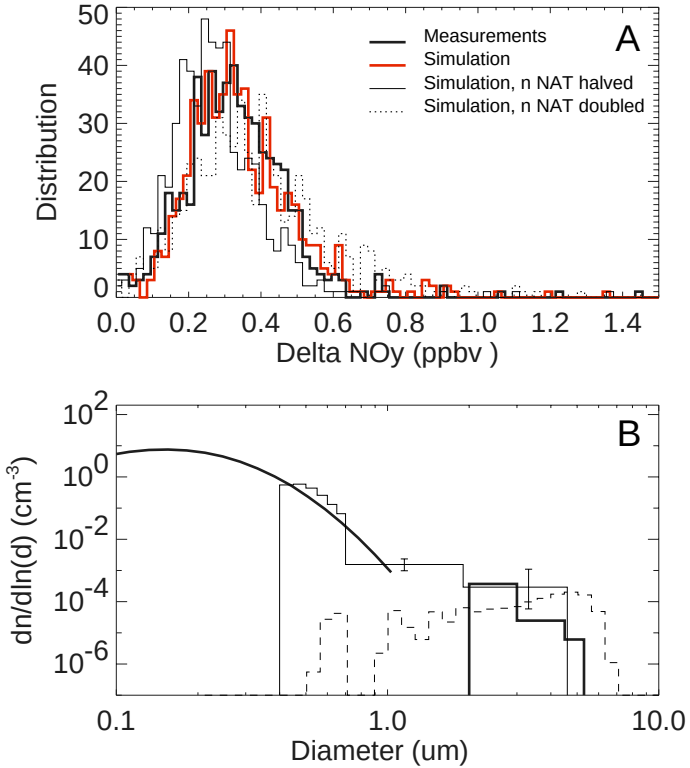

Fig. 3.

ACPD
4, 8579–8607, 2004

Nitric acid trihydrate (NAT) formation at low NAT supersaturations

C. Voigt et al.

(A) Fit of the results of the Monte Carlo simulations (red line) to the occurrence histogram of a 600 s long sequence of NO_y data taken near 14.65 h UT (thick black line). Number density and width of the size classes of NAT particles has been varied in the simulations to fit the occurrence histogram of the NO_y data. Sensitivity studies have been performed either halving (thin black line) or doubling the NAT number density (dashed line), both leading to significant deteriorations of the fit. **(B)** Particle size distribution (thick black lines) at 18.3 km altitude derived from the Monte Carlo simulations of the NO_y data. The large mode of the particle size distribution consists of NAT particles with $2\,\mu m < d < 5.5\,\mu m$ at a number density of $1.6\times10^{-4}\,cm^{-3}$. The error in the NAT number density is ± a factor of 2, as derived from the simulations. The small mode of the particle size distribution shows the ternary background aerosol distribution with a median diameter of 0.17 μm containing 0.03 ppbv HNO_3. For comparison, thin black line shows particle size distribution measured by the FSSP. The error bars indicate the 96% confidence levels. The dashed line shows the NAT particle size distribution simulated with the DLAPSE model (Carslaw et al., 2002) near the flight track between 410 to 430 K potential temperature in a region of 66–69° latitude north and 12–16° longitude east.

ACPD

4, 8579–8607, 2004

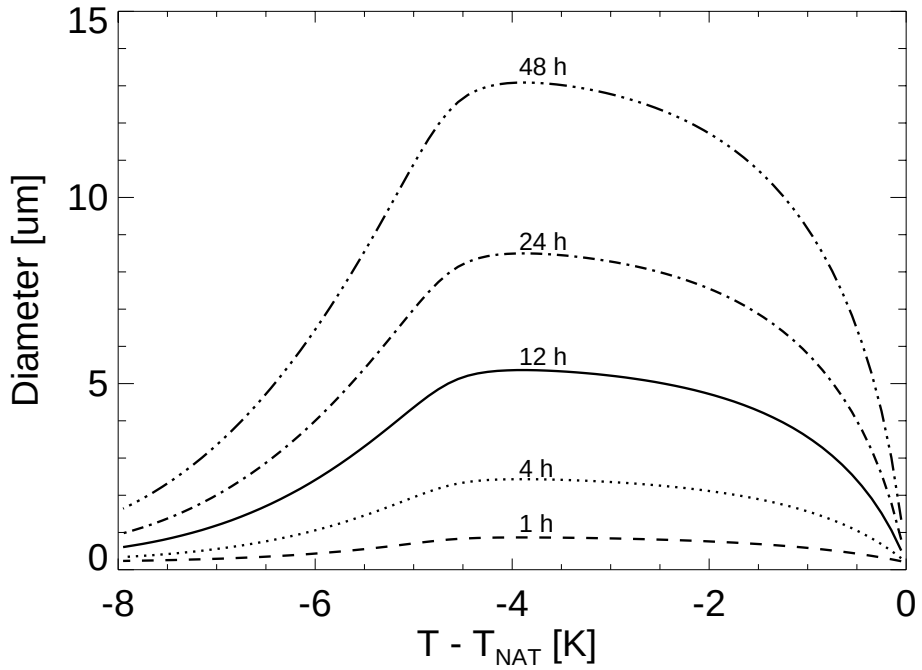

Fig. 4. Box model calculation of NAT particle growth for 10 ppbv total HNO_3 and 5 ppmv H_2O at 50 hPa as a function of the temperature difference with respect to T_{NAT}. The black lines show NAT particle diameters for different growth times between 1 h and 2 days. The deceleration of NAT growth at very low temperatures results from gas phase depletion of nitric acid due to the uptake by ternary aerosol droplets.

ACPD
4, 8579–8607, 2004

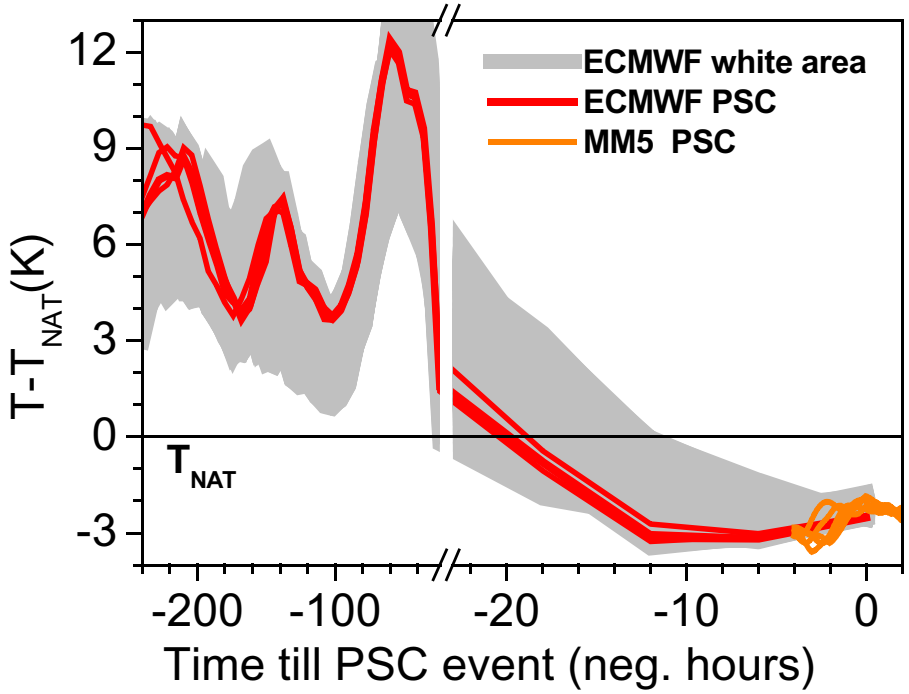

Fig. 5. $T - T_{NAT}$ along 3-D backward trajectories based on 6-h T511/L60 ECMWF operational analysis (red lines and grey shading) and trajectories calculated with the mesoscale MM5 model (Dörnbrack et al., 1999) (orange lines). Grey shading shows the ensemble of all trajectories ending on 6 February at 12:00 UT inside the white box marked in Fig. 1 on a 0.5°×0.5° lat/long grid at 70 hPa. Red and orange lines are trajectories ending at the Geophysica flight path during times of PSC detection at 70 hPa pressure altitude. T_{NAT} has been calculated from the measured NO_y and water vapor profiles. A similar analysis has been performed for the return flight (not shown here).

ACPD
4, 8579–8607, 2004